NASA TECHNICAL NOTE

NASA TN D-2418

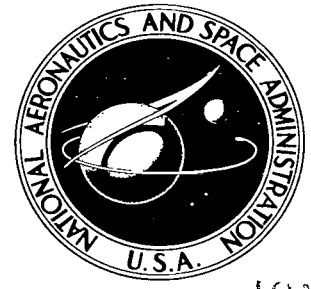

A STUDY OF THE EFFECTIVENESS OF VARIOUS METHODS OF VIBRATION REDUCTION ON SIMPLIFIED SCALE MODELS OF THE NIMBUS SPACECRAFT

by Huey D. Carden and Robert W. Herr

Langley Research Center
Langley Station, Hampton, Va.

NATIONAL AERONAUTICS AND SPACE ADMINISTRATION • WASHINGTON, D. C. • AUGUST 1964

A STUDY OF THE EFFECTIVENESS OF VARIOUS METHODS OF VIBRATION REDUCTION ON SIMPLIFIED SCALE MODELS OF THE NIMBUS SPACECRAFT

By Huey D. Carden and Robert W. Herr

Langley Research Center
Langley Station, Hampton, Va.

NATIONAL AERONAUTICS AND SPACE ADMINISTRATION

For sale by the Office of Technical Services, Department of Commerce,
Washington, D.C. 20230 -- Price $0.75

A STUDY OF THE EFFECTIVENESS OF VARIOUS METHODS OF VIBRATION REDUCTION ON SIMPLIFIED SCALE MODELS OF THE NIMBUS SPACECRAFT

By Huey D. Carden and Robert W. Herr
Langley Research Center

SUMMARY

The results of an experimental investigation of the effectiveness of various isolation and damping methods in reducing the dynamic response of simplified scaled models of the Nimbus spacecraft to vibratory inputs are presented. Experimental mode shapes and natural frequencies of the simulated solar panels were determined and found to compare well with calculated values. Appreciable reductions of structural responses to vibratory-input motions were measured for independent inputs along the roll, pitch, and yaw axes for the cases in which distributed damping and/or isolation was utilized. A comparison of the response of the model with the full-scale spacecraft for inputs along the pitch axis is presented. Also included are the effects of stiffness between the control and sensory sections on the response of the model to vibratory inputs.

INTRODUCTION

The high reliability demanded of spacecraft requires that these complex structures be capable of operation during and after exposure to many hostile environments. Earliest of the environmental hazards encountered, and in many cases the most severe, are the extreme vibration levels through which these payloads pass during the launch and boost phases of the flight sequence. Designing a spacecraft whose natural frequencies are such that it does not respond to the booster inputs is virtually impossible; therefore, it becomes necessary that techniques and structural assembly procedures be developed to reduce the severity of the many resonant conditions which exist in the spacecraft and its component parts.

At the present time, in the design and development stage is a wide variety of spacecraft for which onboard instrumentation is designed for operation on power generated by solar cells mounted on large flexible panels. Vibration tests of prototype spacecraft of this type, at levels well below anticipated flight levels, have resulted in damage to both payloads and associated instrumentation. It is anticipated that future payloads of similar design will experience the same vibration amplification problems unless adequate guidelines are

established for the use of vibration absorbers and structural damping materials in spacecraft design and construction.

The purpose of this paper is to report the results of an experimental investigation which utilized a 1/5-scale model and 1/2-scale dynamic model of the Nimbus spacecraft for evaluating the effectiveness of various isolation and damping methods in reducing the dynamic response of the spacecraft to vibratory inputs. The results presented include both experimental and analytical mode shapes and natural frequencies of the solar panels for the 1/2-scale model, along with the dynamic responses of the 1/5- and 1/2-scale models, and show the effects of damping and isolation at various locations in reducing the structural amplifications and undesirable vibratory motions.

SYMBOLS

C/C_c damping ratio

D panel flexural rigidity, $E\left[\frac{(2h + t)^3 - t^3}{12}\right]$, in-lb

$\overline{D} = \frac{D}{D_r}$

E Young's modulus of elasticity, $lb/in.^2$

f frequency, cps

g acceleration due to gravity at surface of earth, $in./sec^2$

h panel skin thickness, in.

K number of moving mass points on solar-panel planform

k stiffness between control and sensory sections, lb/in.

L length of solar panel, in.

m mass per unit area of panel, $lb\text{-}sec^2/in.^3$

$\overline{m} = \frac{m}{m_r}$

N grid-point number

n number of cycles

R number of unknown deflections left in expression for energy after conditions of constraint have been applied

T total number of points on solar-panel planform

t core thickness of panel section, in.

x_n amplitude of nth cycle

x_o initial amplitude

α weighting number for approximate integration of potential energy of plate

δ damping factor, $\frac{1}{n} \log_e \frac{x_o}{x_n}$

ϵ horizontal distance between vertical grid lines on panel planform

λ vertical distance between horizontal grid lines on panel planform

μ Poisson's ratio

Subscripts:

c calculated values

e experimental values

N,W,NN,EE,. . .NE/2 directional bearings of grid points with respect to a general central point

O evaluation of a quantity at a general grid point

r any convenient reference of a quantity

APPARATUS AND TEST PROCEDURE

Vibration tests were conducted on two models patterned after the Nimbus spacecraft. One was a 1/5-scale model and the other, a 1/2-scale dynamic model. The 1/5-scale model was a preliminary model to provide quantitative guidelines for exploring potential problems with more sophisticated models and to assess the improvement, if any, to be expected when various isolation or damping methods were employed. The 1/2-scale model was investigated more thoroughly, and more consideration was given to details in the structure. Photographs and sketches of the spacecraft and of the models and testing apparatus are given in figures 1 to 7.

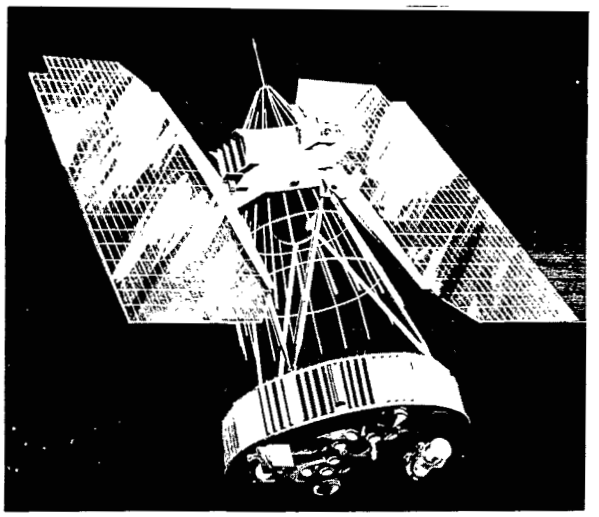

L-64-4702

Figure 1.- Nimbus spacecraft.

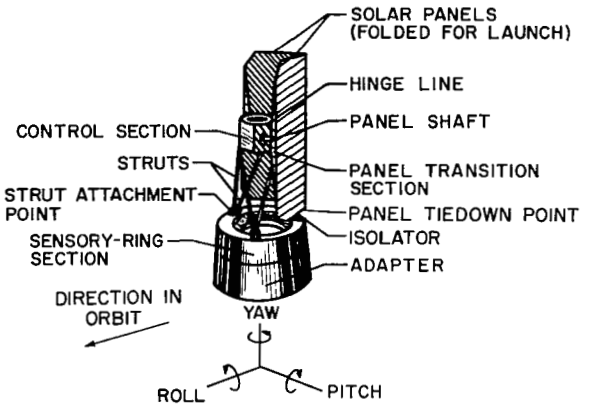

Figure 2.- General configuration and elements of Nimbus.

1/5-Scale Model

Description of model.- The general configuration of the solar panels, control section, and the struts of the 1/5-scale model (fig. 3) was similar to that of the Nimbus spacecraft in figure 1, but no attempt was made to scale the mass and stiffness. The bottom ends of the struts were attached to an 11-inch-diameter aluminum plate, 1/4 inch thick, which replaced the sensory section. Provisions were also made to allow different commercial rubber isolators to be used at the strut attachment points. Two sets of solar panels were tested. One set was cut from 0.032-inch aluminum, and the other set utilized a sandwich construction consisting of two sheets of 0.016-inch aluminum bonded together with a viscoelastic adhesive.

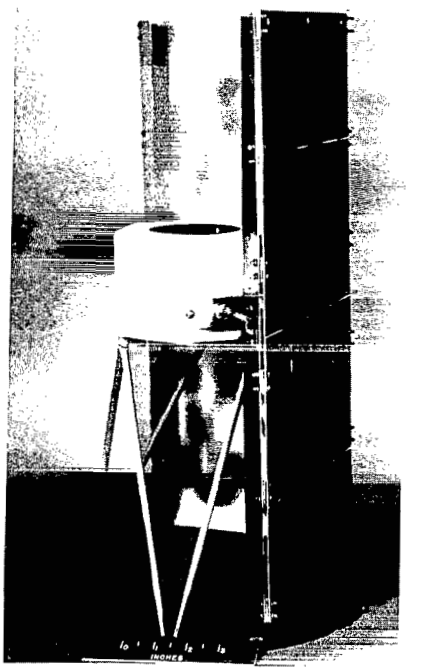

L-63-5911

Figure 3.- General configuration of 1/5-scale model of Nimbus spacecraft.

Instrumentation.- Excitation was provided by a 10-pound-force electromagnetic shaker. Input accelerations at the shaker attachment points and the resulting model responses were measured with crystal accelerometers. Signals from the accelerometers were routed through cathode followers to true root-mean-square (rms) voltmeters. Voltages measured on the meters were recorded along with the excitation frequency which was measured with a frequency-period counter.

Test procedure.- Excitation of the model was applied along the roll and yaw axes through the 1/4-inch base plate or sensory section. The input accelerations were measured on the base plate adjacent to one of the strut attachment points.

Output accelerations as a function of frequency were measured at various locations on one of the solar panels in the direction normal to the surface of the panel. Accelerations were also measured on a shelf bracket located on the side of the control section.

Accelerations were measured on the 0.032-inch-thick set of aluminum simulated solar panels, hereinafter referred to as solid panels, for three strut-attachment configurations. These configurations are: (1) rigid attachment; (2) three isolators with an axial stiffness of 8 lb/in. and a radial stiffness of 30 lb/in. and which are hereinafter referred to as 8-30 isolators; (3) three isolators with an axial and radial stiffness both equal to 68 lb/in. and which are hereinafter referred to as 68-68 isolators. (See ref. 1.) The panels were then replaced by a sandwich-construction configuration and the process was repeated.

1/2-Scale Dynamic Model

Description of model.- The construction of the 1/2-scale model (fig. 4) was a simplified version of the full-scale Nimbus. The bending stiffness of the solar panels, panel shaft, and struts, as well as the mass of all the major components, was approximately scaled. Unlike the 1/5-scale model, the 1/2-scale model had a simulated sensory section and adapter section. Two sets of solar

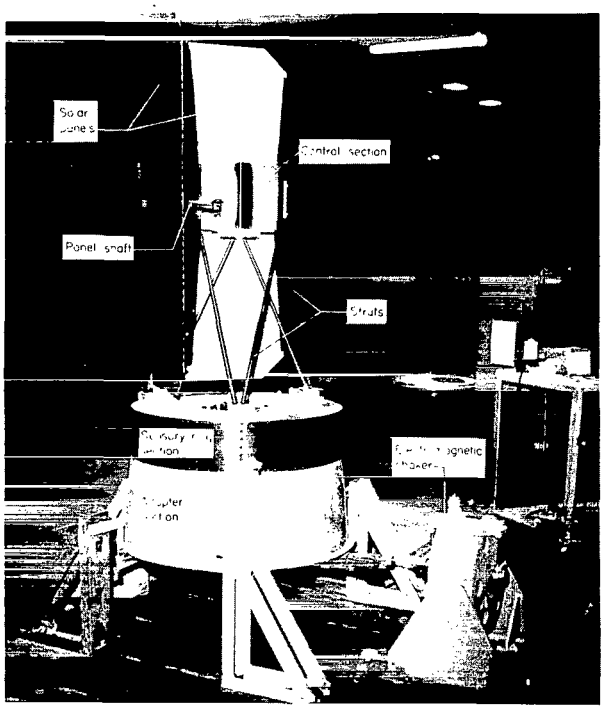

L-63-5913.1
Figure 4.- One-half-scale model of Nimbus mounted on suspension system with electromagnetic shaker attached.

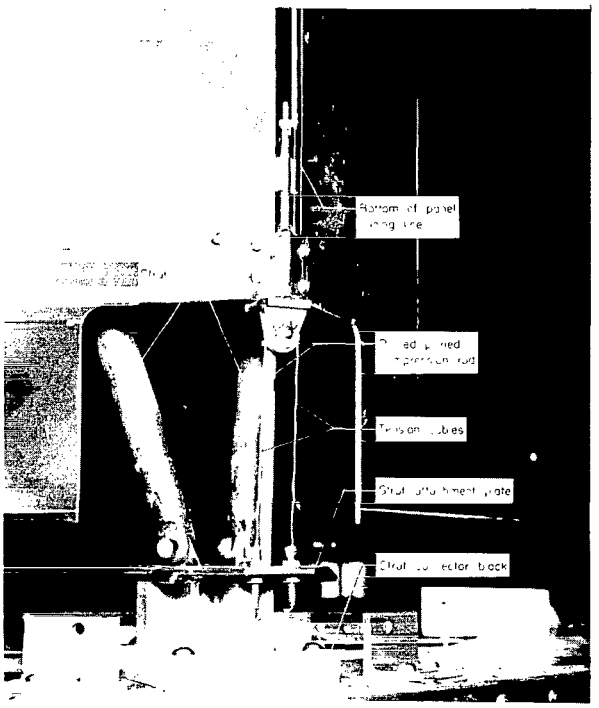

L-62-8193.1
Figure 5.- Details of solar-panel tiedown assembly of 1/2-scale Nimbus model.

panels were fabricated. Both consisted of two sheets of 0.016-inch aluminum attached to a tapered balsa-wood core. The taper of the wood core varied linearly from 0.0625 inch at the horizontal center line of the panel to 0.020 inch at the panel tip. In this manner it was possible to obtain the desired stiffness distribution. In one set, the aluminum sheets were bonded to the wood core with an epoxy cement, whereas in the other set the sheets were bonded with a viscoelastic adhesive which provided shear damping. The panel tiedown for the folded panel configuration (fig. 5) was similar to that of the full-scale Nimbus. The pinned-pinned compression rod in conjunction with the tension cables allowed the panels limited freedom of movement in essentially all directions, except for relative movement between the bottom of the panel joining line and the strut attachment plate. Figure 6 presents the principal dimensions of the 1/2-scale model, and table I gives a weight distribution of the major model components and a comparison with the desired 1/2-scale values.

TABLE I.- WEIGHT DISTRIBUTION OF 1/2-SCALE DYNAMIC MODEL

OF NIMBUS SPACECRAFT

Model section	Weight distribution, lb			
	1/2-scale model		Basic model structure	Simulated instruments ballast
	Desired	Actual		
Control	16.50	16.24	3.62	12.62
Sensory	58.00	60.55	10.09	50.46
Struts	1.10	3.43	3.43	
Bonded panels	[a]7.25	[a]8.02	8.02	
Damped panels	[a]7.25	[a]8.20	8.20	
Adapter	8.00	2.96	2.96	
Total weight	90.85	99.40		

[a]Two panels.

COMPONENT SIZE	DIMENSION, IN.
A - CONTROL-BOX WIDTH	11
B - SOLAR-PANEL WIDTH	19.2
C - SOLAR-PANEL LENGTH	48
D - OVERALL LENGTH, INCLUDING ADAPTER	69
E - SENSORY-RING HEIGHT	6.5
F - SPACECRAFT-ADAPTER HEIGHT	12
G - SENSORY-RING DIAMETER	29.5
H - SPACECRAFT-ADAPTER DIAMETER (BOTTOM)	30

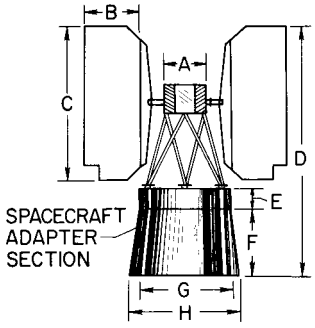

Figure 6.- Principal dimensions of 1/2-scale Nimbus model.

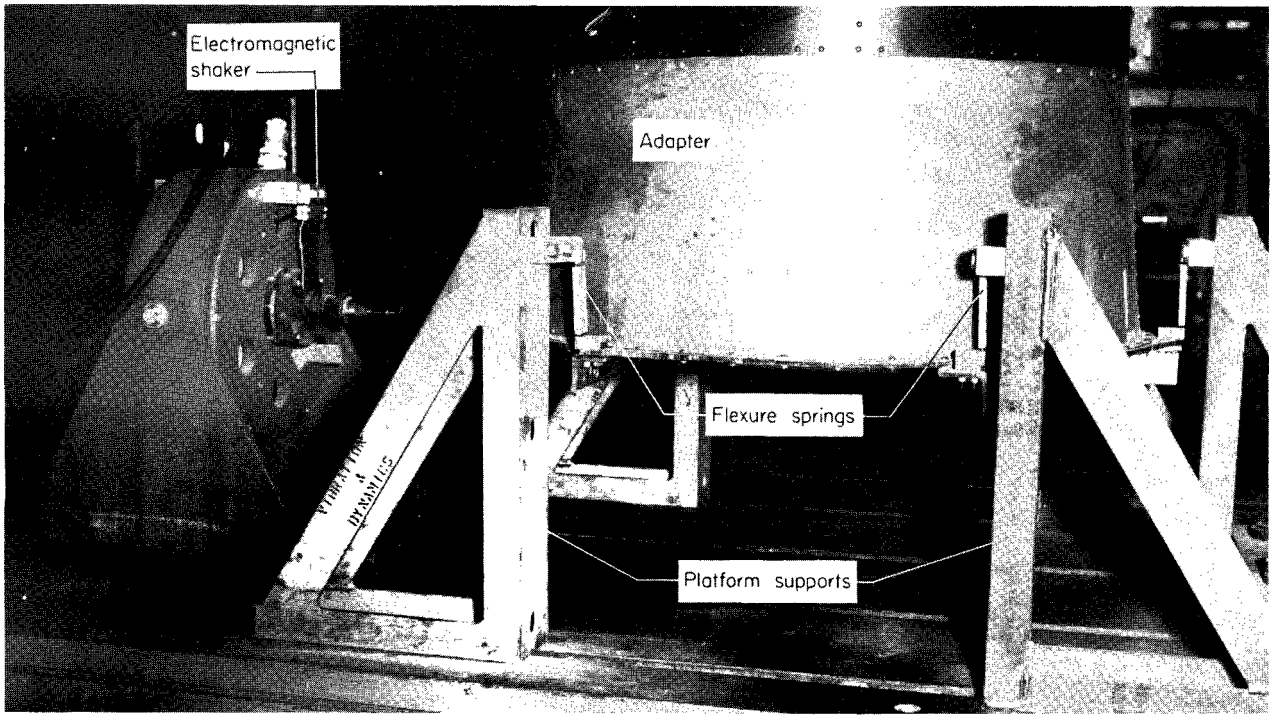

L-63-5914.1

Figure 7.- Model-mounting platform suspended on steel flexure springs.

Instrumentation.- For the tests, excitation of the 1/2-scale model was provided by a 50-pound-force electromagnetic shaker. In order to minimize the undesirable effects on the responses and modes of the model which can result from the added mass of acceleration pickups, accelerometers weighing only 0.026 ounce were utilized. The useful frequency range of the accelerometers was from 3 cps to 4000 cps. Accelerometer output signals were routed through cathode followers to the true rms voltmeters, which were accurate within 10 percent at a frequency of 5 cps. As for the tests, of the 1/5-scale model, the excitation frequency was measured by a frequency-period counter.

Test procedure.- For tests involving excitation along the roll and pitch axes, the 1/2-scale Nimbus model was mounted on a platform which was suspended on steel flexure springs (fig. 7) to provide essentially planar motions. The model was then vibrated through a frequency range to determine the effects of different damping and/or isolation methods. For tests in which the excitation was parallel to the yaw axis, the model was suspended by nylon ropes attached at the center of gravity of the combination of the control section, struts, and solar panels, and at the center of gravity of the combination of the sensory system and adapter. For excitation along each axis, responses of the model to the input motions were measured at various locations on the solar panels, control section, and in several compartments around the sensory system.

PRESENTATION AND DISCUSSION OF RESULTS

1/5-Scale Model

Typical results obtained from the preliminary tests with the 1/5-scale model are given in figures 8 and 9. For excitation along the roll or yaw axes, amplification factors were measured on a shelf on the side of the control section and on the solid and sandwich solar panels for two stiffnesses of isolation mounts, as well as for the rigid-attachment case, for which the struts were bolted directly to the base plate. The amplification factor is defined as the ratio of the output acceleration to the input acceleration. The results indicate that the structural amplifications on the panel locations (figs. 8, 9(a), and 9(b)) and on the shelf in the control section (figs. 9(c) and 9(d)) were numerous and usually large throughout the frequency range of excitation. The use of the damped panels and isolators resulted in greatly reduced magnitudes or complete elimination of the structural amplifications (note the solid symbols) for most of the locations considered. The natural frequencies of the control section and panels translating on the 8-30 and 68-68 isolators were 16.4 cps and 35 cps, respectively, whereas the rocking frequencies on these mounts along the roll direction were 5 cps and 8 cps, respectively. The minimum resonant frequency of the panels was approximately 35 cps.

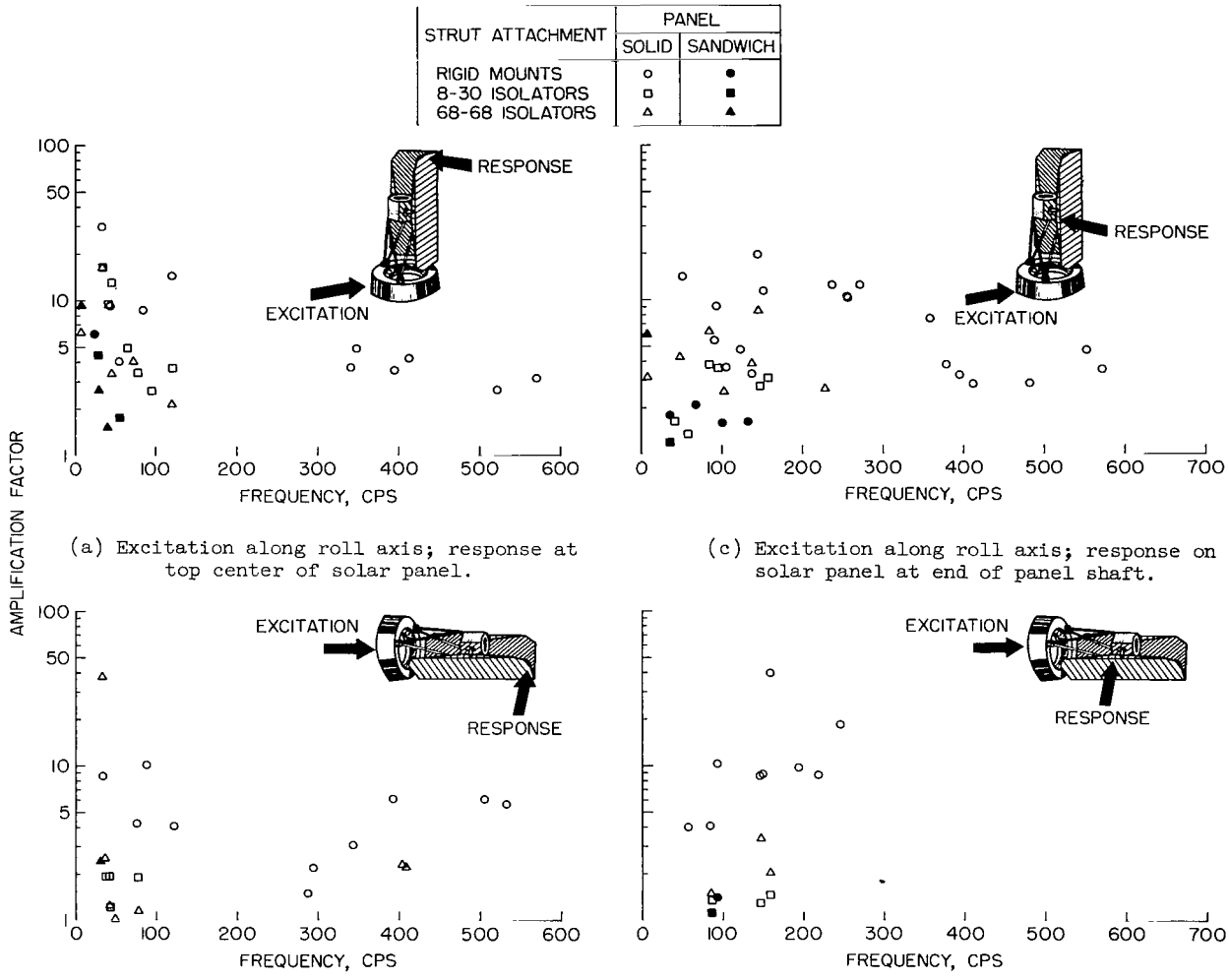

(a) Excitation along roll axis; response at top center of solar panel.

(c) Excitation along roll axis; response on solar panel at end of panel shaft.

(b) Excitation along yaw axis; response at top center of solar panel. (Note: Values for model with rigid mounts and sandwich panels and for model with 8-30 isolators and sandwich panels are less than 1 for all frequencies.)

(d) Excitation along yaw axis; response on solar panel at end of panel shaft. (Note: Values for model with 68-68 isolators and sandwich panels are less than 1 for all frequencies.)

Figure 8.- Dynamic amplification as a function of excitation frequency for 1/5-scale Nimbus model.

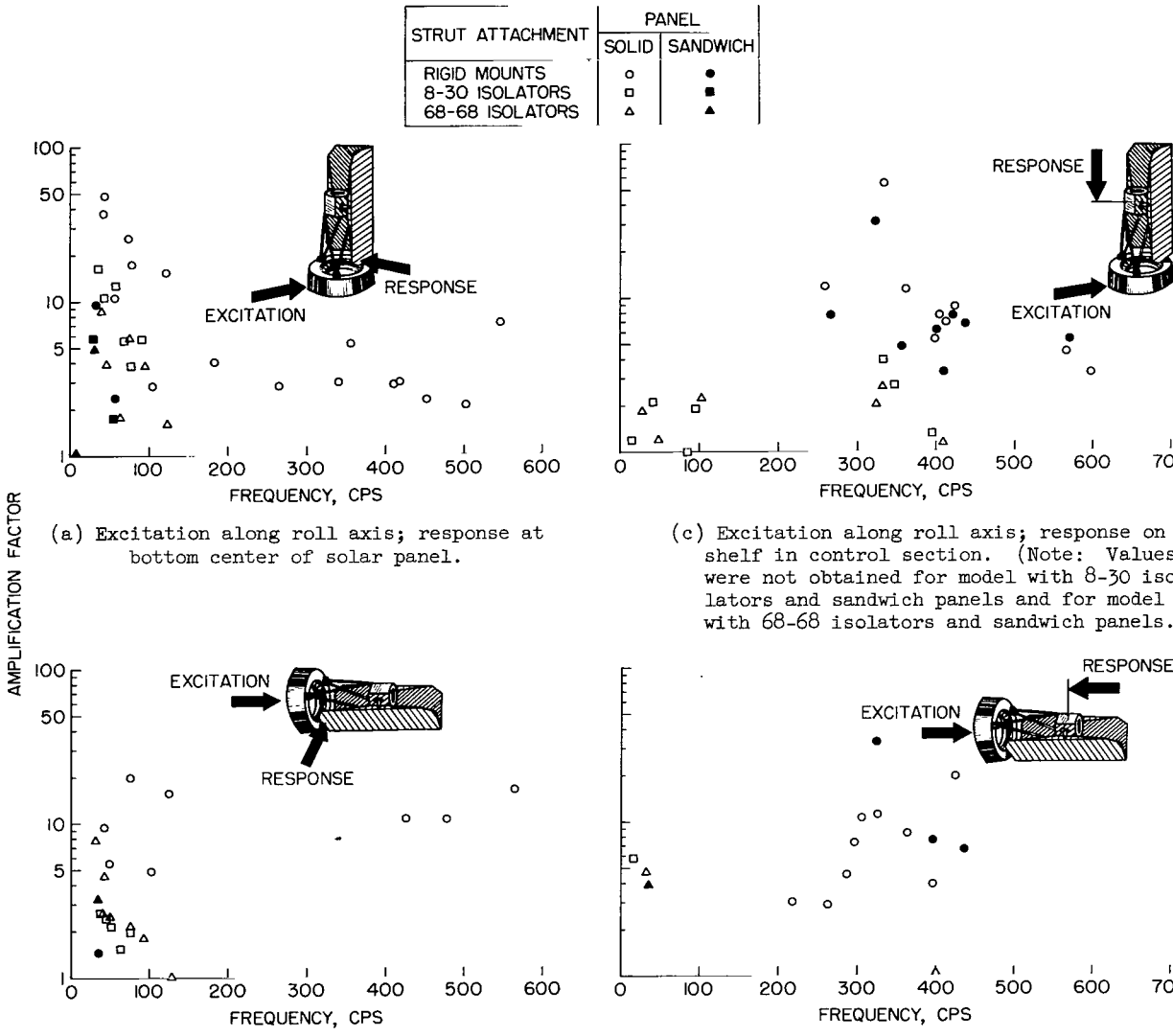

(a) Excitation along roll axis; response at bottom center of solar panel.

(c) Excitation along roll axis; response on shelf in control section. (Note: Values were not obtained for model with 8-30 isolators and sandwich panels and for model with 68-68 isolators and sandwich panels.

(b) Excitation along yaw axis; response at bottom center of solar panel. (Note: values for model with 8-30 isolators and sandwich panels are less than 1 for all frequencies.)

(d) Excitation along yaw axis; response on shelf in control section. (Note: Values were not obtained for model with 8-30 isolators and sandwich panels.)

Figure 9.- Dynamic amplification as a function of excitation frequency for 1/5-scale Nimbus model.

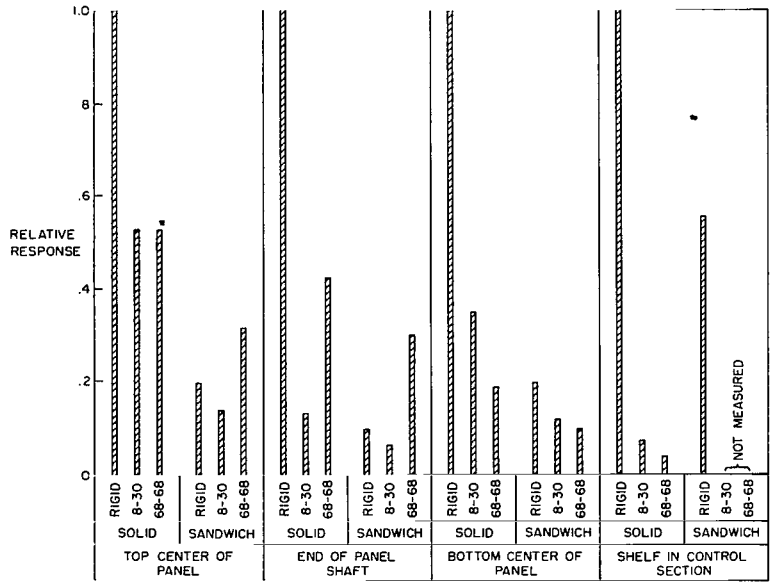

(a) Excitation along roll axis.

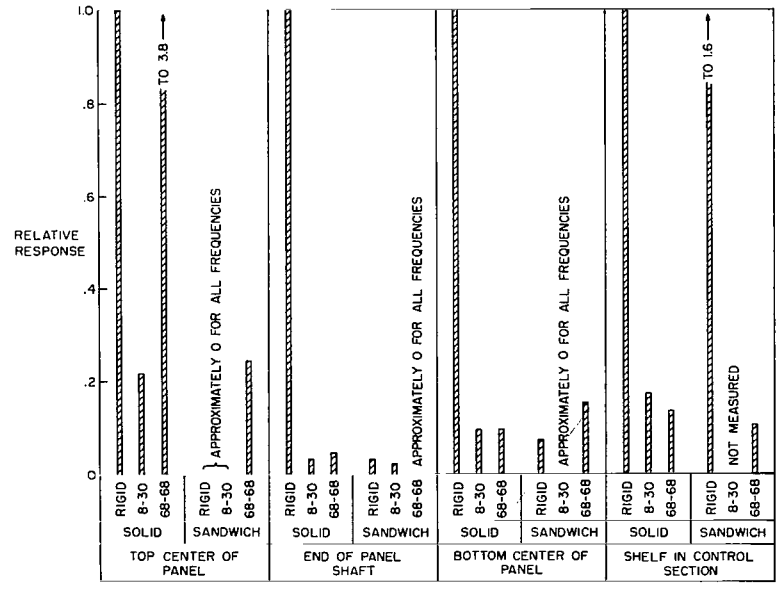

(b) Excitation along yaw axis.

Figure 10.- Summary of relative effectiveness of isolation and damping methods in reducing amplification factors on 1/5-scale Nimbus model.

The data shown in figures 8 and 9 are summarized in figure 10. The ordinate of figure 10 shows the relative response for the various methods employed, and the abscissa gives the combination of approaches utilized in an attempt to reduce or alleviate structural amplifications and the position at which the amplifications were measured. The relative response was determined by normalizing maximum amplification values measured in each case on the value of the maximum amplification factors measured for the solid panels and rigid mounts. For excitation along the roll axis, the sandwich-construction solar panels were usually more effective in reducing the maximum structural amplifications than were the isolators with the solid panels. The combination of the isolators and the sandwich panels, however, was the most effective on the 1/5-scale model. When excitation was applied along the yaw axis, both sets of isolators and/or the damped sandwich panels were effective in reducing the magnitudes of the detectable structural resonances. The only exceptions noted were for the 68-68 isolators for the top center of the solid panel and for the sandwich panels on rigid mounts, for the location on the shelf in the control section. (See fig. 10(b).)

The results from the preliminary tests indicated potential vibration problems which should be explored by the use of more sophisticated models of Nimbus. The results also indicated that appreciable reductions in the magnitude of structural resonances could possibly be realized on the 1/2-scale Nimbus model through the use of appropriate damping and/or isolation.

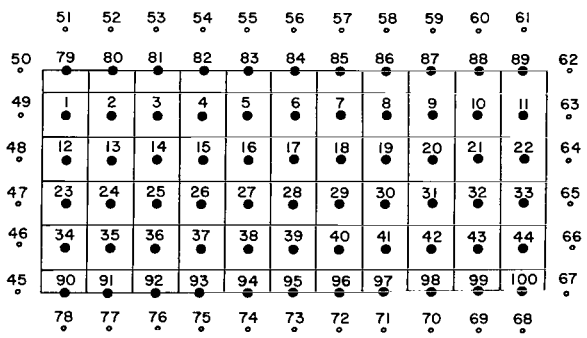

(a) Stations for finite-difference calculations of frequencies for type 1 integration. K = 44; R = 78; T = 100.

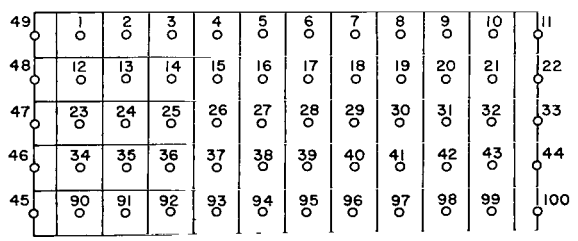

(b) Stations for type 2 integration.

Figure 11.- Planform assumed for panel for calculating frequencies and mode shapes by method of reference 2.

1/2-Scale Dynamic Model

Panel frequencies and mode shapes.- Concurrent with the experimental determination of the amplification factors of the 1/2-scale Nimbus model, an analytical technique for calculating the modes and frequencies of the simulated solar panels was employed. The technique utilizes a general finite-difference method in calculating the simple harmonic flexures of plates. The basis of the technique, along with the procedure for application of the method to plate-vibration problems, is fully discussed in reference 2. Figure 11 gives the planforms of the Nimbus panel for hinged-hinged edge conditions along the length of the panel. Table II gives the computing-machine inputs for calculating the panel modes and frequencies.

TABLE II.- COMPUTING-MACHINE INPUT FOR CALCULATION OF MODES AND FREQUENCIES OF SOLAR PANEL FOR HINGED-HINGED EDGES ALONG PANEL LENGTH

[L = 48 in.; ϵ/λ = 1.136; μ = 0.333; K = 44; R = 78; T = 100; D_r = 428 in-lb; m_r = 0.00083 (lb-sec^2)/in.]

(1) Grid-point number	(2) $\overline{D}_0 a_0$	(3) $\overline{D}_{NE} a^2_{NE}/2$	(4) N_{NN}	(5) N_{NW}	(6) N_N	(7) N_{NE}	(8) N_{WW}	(9) N_W	(10) N_O	(11) N_E	(12) N_{EE}	(13) N_{SW}	(14) N_S	(15) N_{SE}	(16) N_{SS}	(17) $\overline{m}_0 a_0$
1	0.297	0.297	51	50	79	80	0	49	1	2	3	48	12	13	23	1
2	.474	.474	52	79	80	81	49	1	2	3	4	12	13	14	24	1
3	.650	.650	53	80	81	82	1	2	3	4	5	13	14	15	25	1
4	.827	.827	54	81	82	83	2	3	4	5	6	14	15	16	26	1
5	1.000	1.000	55	82	83	84	3	4	5	6	7	15	16	17	27	1
6	1.000	1.000	56	83	84	85	4	5	6	7	8	16	17	18	28	1
7	1.000	.827	57	84	85	86	5	6	7	8	9	17	18	19	29	1
8	.827	.650	58	85	86	87	6	7	8	9	10	18	19	20	30	1
9	.650	.474	59	86	87	88	7	8	9	10	11	19	20	21	31	1
10	.474	.297	60	87	88	89	8	9	10	11	63	20	21	22	32	1
11	.297	.1485	61	88	89	62	9	10	11	63	0	21	22	64	33	1
12	.297	.297	79	49	1	2	0	48	12	13	14	47	23	24	34	1
13	.474	.474	80	1	2	3	48	12	13	14	15	23	24	25	35	1
14	.650	.650	81	2	3	4	12	13	14	15	16	24	25	26	36	1
15	.827	.827	82	3	4	5	13	14	15	16	17	25	26	27	37	1
16	1.000	1.000	83	4	5	6	14	15	16	17	18	26	27	28	38	1
17	1.000	1.000	84	5	6	7	15	16	17	18	19	27	28	29	39	1
18	1.000	.827	85	6	7	8	16	17	18	19	20	28	29	30	40	1
19	.827	.650	86	7	8	9	17	18	19	20	21	29	30	31	41	1
20	.650	.474	87	8	9	10	18	19	20	21	22	30	31	32	42	1
21	.474	.297	88	9	10	11	19	20	21	22	64	31	32	33	43	1
22	.297	.1485	89	10	11	63	20	21	22	64	0	32	33	65	44	1
23	.297	.297	1	48	12	13	0	47	23	24	25	46	34	35	90	1
24	.474	.474	2	12	13	14	47	23	24	25	26	34	35	36	91	1
25	.650	.650	3	13	14	15	23	24	25	26	27	35	36	37	92	1
26	.827	.827	4	14	15	16	24	25	26	27	28	36	37	38	93	1
27	1.000	1.000	5	15	16	17	25	26	27	28	29	37	38	39	94	1
28	1.000	1.000	6	16	17	18	26	27	28	29	30	38	39	40	95	1
29	1.000	.827	7	17	18	19	27	28	29	30	31	39	40	41	96	1
30	.827	.650	8	18	19	20	28	29	30	31	32	40	41	42	97	1
31	.650	.474	9	19	20	21	29	30	31	32	33	41	42	43	98	1
32	.474	.297	10	20	21	22	30	31	32	33	65	42	43	44	99	1
33	.297	.1485	11	21	22	64	31	32	33	65	0	43	44	66	100	1
34	.297	.297	12	47	23	24	0	46	34	35	36	45	90	91	78	1
35	.474	.474	13	23	24	25	46	34	35	36	37	90	91	92	77	1
36	.650	.650	14	24	25	26	34	35	36	37	38	91	92	93	76	1
37	.827	.827	15	25	26	27	35	36	37	38	39	92	93	94	75	1
38	1.000	1.000	16	26	27	28	36	37	38	39	40	93	94	95	74	1
39	1.000	1.000	17	27	28	29	37	38	39	40	41	94	95	96	73	1
40	1.000	.827	18	28	29	30	38	39	40	41	42	95	96	97	72	1
41	.827	.650	19	29	30	31	39	40	41	42	43	96	97	98	71	1
42	.650	.474	20	30	31	32	40	41	42	43	44	97	98	99	70	1
43	.474	.297	21	31	32	33	41	42	43	44	66	98	99	100	69	1
44	.297	.1485	22	32	33	65	42	43	44	66	0	99	100	67	68	1
45	0	.1485	47	0	46	34	0	0	45	90	91	0	0	78	0	
46	0	.1485	48	0	47	23	0	0	46	34	35	0	45	90	0	
47	0	.1485	49	0	48	12	0	0	47	23	24	0	46	34	45	
48	0	.1485	50	0	49	1	0	0	48	12	13	0	47	23	46	
49	0	.1485	0	0	50	79	0	0	49	1	2	0	48	12	47	
50	0	0	0	0	0	51	0	0	50	79	80	0	49	1	48	

(1) Grid-point number	(2) $\overline{D}_0 a_0$	(3) $\overline{D}_{NE} a^2_{NE}/2$	(4) N_{NN}	(5) N_{NW}	(6) N_N	(7) N_{NE}	(8) N_{WW}	(9) N_W	(10) N_O	(11) N_E	(12) N_{EE}	(13) N_{SW}	(14) N_S	(15) N_{SE}	(16) N_{SS}	(17) $\overline{m}_0 a_0$
51	0	0	0	0	0	0	0	0	51	52	53	50	79	80	1	
52	0	0	0	0	0	0	0	51	52	53	54	79	80	81	2	
53	0	0	0	0	0	0	51	52	53	54	55	80	81	82	3	
54	0	0	0	0	0	0	52	53	54	55	56	81	82	83	4	
55	0	0	0	0	0	0	53	54	55	56	57	82	83	84	5	
56	0	0	0	0	0	0	54	55	56	57	58	83	84	85	6	
57	0	0	0	0	0	0	55	56	57	58	59	84	85	86	7	
58	0	0	0	0	0	0	56	57	58	59	60	85	86	87	8	
59	0	0	0	0	0	0	57	58	59	60	61	86	87	88	9	
60	0	0	0	0	0	0	58	59	60	61	0	87	88	89	10	
61	0	0	0	0	0	0	59	60	61	0	0	88	89	62	11	
62	0	0	0	61	0	0	88	89	62	0	0	11	63	0	64	
63	0	0	0	89	62	0	10	11	63	0	0	22	64	0	65	
64	0	0	62	11	63	0	21	22	64	0	0	33	65	0	66	
65	0	0	63	22	64	0	32	33	65	0	0	44	66	0	67	
66	0	0	64	33	65	0	43	44	66	0	0	100	67	0	0	
67	0	0	65	44	66	0	99	100	67	0	0	68	0	0	0	
68	0	0	44	99	100	67	70	69	68	0	0	0	0	0	0	
69	0	0	43	98	99	100	71	70	69	68	0	0	0	0	0	
70	0	0	42	97	98	99	72	71	70	69	68	0	0	0	0	
71	0	0	41	96	97	98	73	72	71	70	69	0	0	0	0	
72	0	0	40	95	96	97	74	73	72	71	70	0	0	0	0	
73	0	0	39	94	95	96	75	74	73	72	71	0	0	0	0	
74	0	0	38	93	94	95	76	75	74	73	72	0	0	0	0	
75	0	0	37	92	93	94	77	76	75	74	73	0	0	0	0	
76	0	0	36	91	92	93	78	77	76	75	74	0	0	0	0	
77	0	0	35	90	91	92	0	78	77	76	75	0	0	0	0	
78	0	0	34	45	90	91	0	0	78	77	76	0	0	0	0	
79	.1485	0														
80	.237	0														
81	.325	0														
82	.4135	0														
83	.500	0														
84	.500	0														
85	.500	0														
86	.4135	0														
87	.325	0														
88	.237	0														
89	.1485	0														
90	.1485	.297														
91	.237	.474														
92	.325	.650														
93	.4135	.827														
94	.500	1.000														
95	.500	1.000														
96	.500	.827														
97	.4135	.650														
98	.325	.474														
99	.237	.297														
100	.1485	.1485														

Computed frequencies for the first ten modes are compared with experimental results in figure 12, where it can be seen that the agreement, in general, is good. The largest discrepancies occurred for modes four, five, and six. Closer correspondence between all computed and experimental frequencies could possibly be realized by more refined panel-stiffness distribution for input into the computing-machine procedure or by taking into consideration the effect of the panel cutouts.

The dashed lines in figure 12 locate the computed node lines for the panel when the panel is considered to be completely rectangular in form. The actual planform, however, had panel cutouts as indicated by the small shaded areas at three corners of each sketch in figure 12. Substantial agreement, nevertheless, is shown between computed and experimental (solid lines) nodes.

Comparison of model response with full-scale-vehicle response.- In order to obtain an indication of the degree of simulation that was achieved in the 1/2-scale Nimbus, a comparison between the responses of the 1/2-scale model and the full-scale spacecraft was made at the base of the control section for inputs along the pitch axis. The response of the 1/2-scale model is given in figure 13 by the dashed line and open symbols; the solid symbols denote the peak values of the measured resonance. Input accelerations to the model were limited by the available shaker force to approximately 83 percent of the desired 0.6g input level. Shown in the figure as a solid line is the corresponding experimentally measured response of the full-scale vehicle. These data were obtained during Nimbus vibration analysis performed by the General Electric Co., Missile and Space Vehicle Department, Valley Forge, Pa., under NASA Contract NAS5-978 to Goddard Space Flight Center. The figure shows that general agreement exists between resonances of the model and the full-scale vehicle in the frequency range up to approximately 35 cps. However, two low-frequency resonant responses, which were not noted on the full-scale Nimbus, were measured on the 1/2-scale model. It is probable that the compromises necessitated in the construction of the model struts and strut attachments may have introduced these additional responses. But it is also possible that the inherent damping in these modes on the full-scale spacecraft was sufficiently high to mask out the individual modal responses.

In an elastic structure, the response of the structure is dependent on the input accelerations and the amplification factors which relate the response of the structure to the input accelerations. For the 1/2-scale model under consideration, the primary interest was the determination of the amplification factors for the spacecraft and the evaluation of the effectiveness of certain methods for attenuating these amplifications.

Effect of damping.- One of the most significant factors which affects the amplification factors is the damping of the structure. In general, any increase in the damping of the structure is beneficial, but the use of damping can be made more effective by distribution of viscoelastic materials in areas of maximum relative shear displacement between two sandwich faces. (See refs. 3 and 4.) Thus, for minimum structural response to a given input spectrum, every attempt should be made to incorporate damping in the structure and to distribute this damping in areas as indicated by the critical modes.

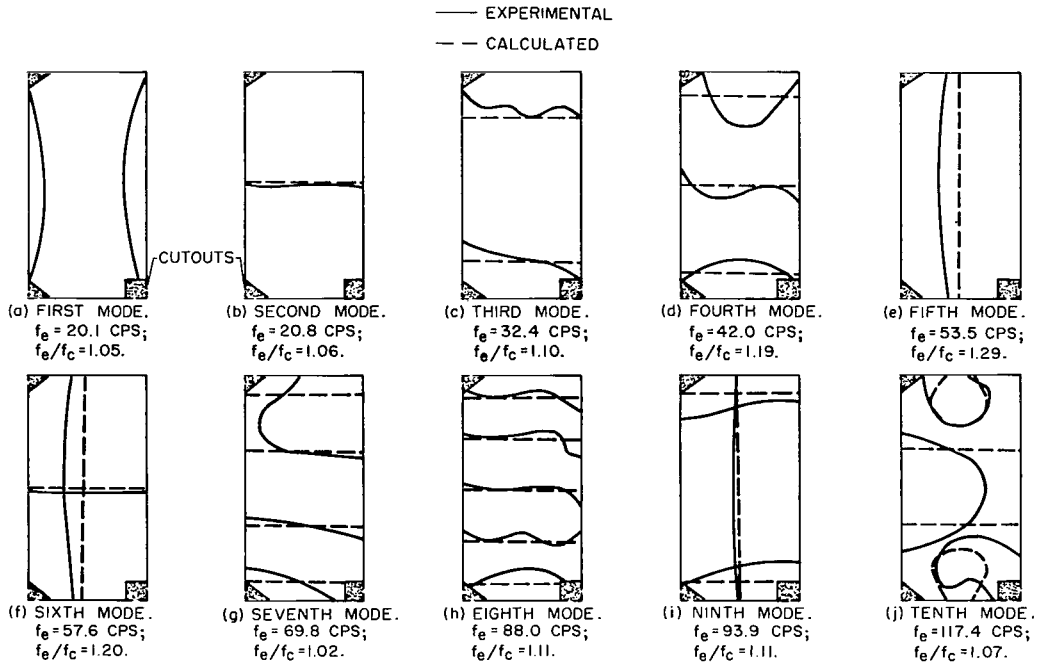

Figure 12.- Comparison of experimental and calculated modes and frequencies of simulated solar panel.

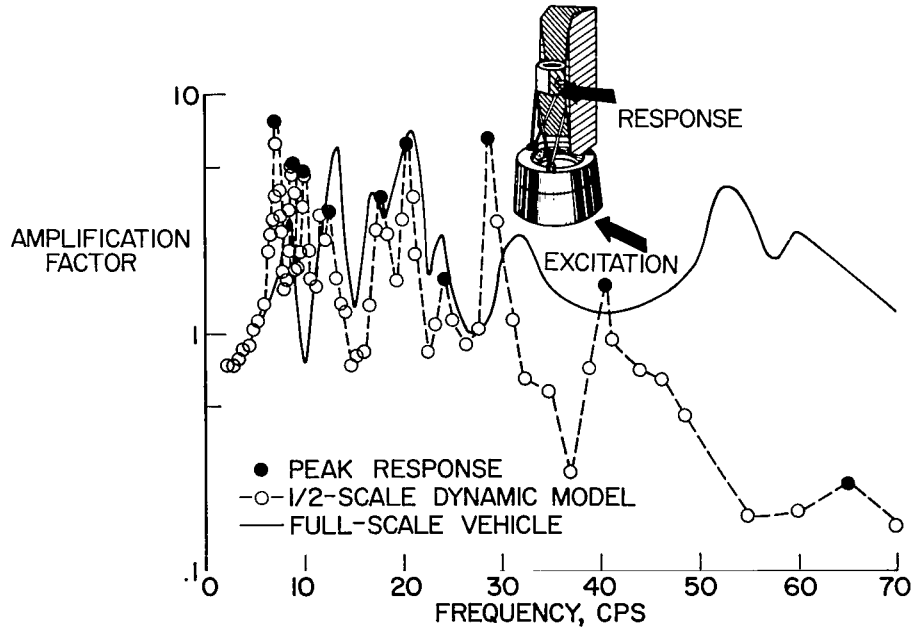

Figure 13.- Comparison between responses at base of control section on 1/2-scale model and full-scale vehicle. Excitation is along pitch axis. (Model frequencies are divided by 2.)

In the use of the two sets of solar panels, the amount of damping present in the oscillatory system was determined by measuring the rate of decay of oscillations for each set. The decay of the oscillation specified by the damping factor δ is defined as

$$\delta = \frac{1}{n} \log_e \frac{x_o}{x_n} = 2\pi \frac{C}{C_c}$$

where n is the number of cycles over which the decay was measured, x_o is the initial amplitude, and x_n is the amplitude after n cycles of oscillation. The value of δ can also be expressed in terms of the critical damping ratio C/C_c. (See ref. 3.) The values for C/C_c for the epoxy-cement bonded panels and the damping-adhesive bonded panels were 0.003 and 0.020, respectively, for the first mode of the panel.

The results of the study of the effects of distributed damping in the solar panels of the 1/2-scale model are given in figures 14 and 15. For excitation along the roll axis, amplification factors were measured at four locations on the model for a stiffness between the control section and the sensory section of $k = 15{,}250$ lb/in. For excitation along the pitch axis (fig. 15), amplification factors were measured at three of the same locations as those shown in figure 14 for excitation along the roll axis. The test results which are presented in figures 14 and 15 emphasize three significant points. The first is that very high amplifications exist in such structures. Second, the many structural resonances were associated mainly with the natural modes of the panels. This fact suggests that proper design of the solar panels may be a means of locating the natural frequencies of the structure in certain areas in the frequency spectrum. In this manner, significant reductions in conditions of resonance between the spacecraft panels and the booster inputs may be feasible. The third point is that the response of such a structure to unsteady forces can be substantially reduced, with only a modest weight increase (table I), by the use of damping materials at suitably chosen points. A comparison of the curves in figures 14 and 15 indicates the relatively high degree of energy dissipation that was attained in the sandwich-construction panels (dashed lines). The added damping was least effective in reducing the amplifications measured at the base of the control section, particularly for excitation along the roll axis. (Fig. 14(d).)

Effects of isolation and damping.- As a further phase of the investigation undertaken with the 1/2-scale Nimbus model, the effects of a combination of isolation and damping on the response of the vehicle to vibratory inputs were conducted. The results of the tests for excitation along the pitch axis in which both isolation mounts and damping were utilized are presented in figures 16 and 17. Two isolation mounts with a maximum axial-load capacity of $12\frac{1}{2}$ pounds were used on the two struts which are located forward of the pitch axis when the vehicle is in orbital attitude (fig. 2). On the strut rearward of the pitch axis for orbital attitude, an isolation mount with a maximum axial-load capacity of 20 pounds was used. The effective maximum radial capacity of the combination was experimentally determined as approximately ± 15.5 pounds.

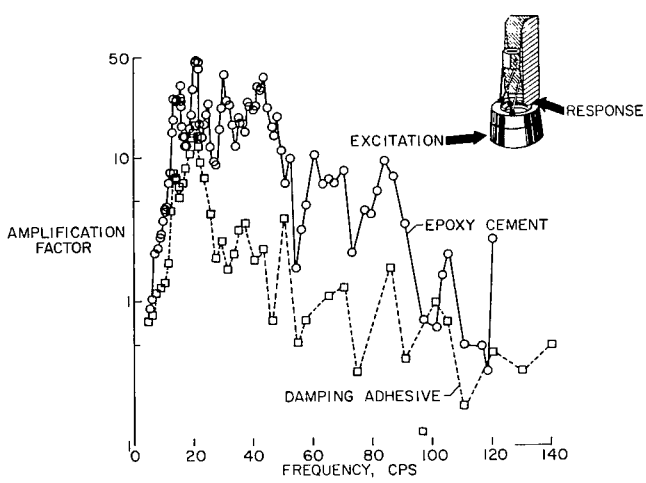

(a) Response at bottom center of solar panel.

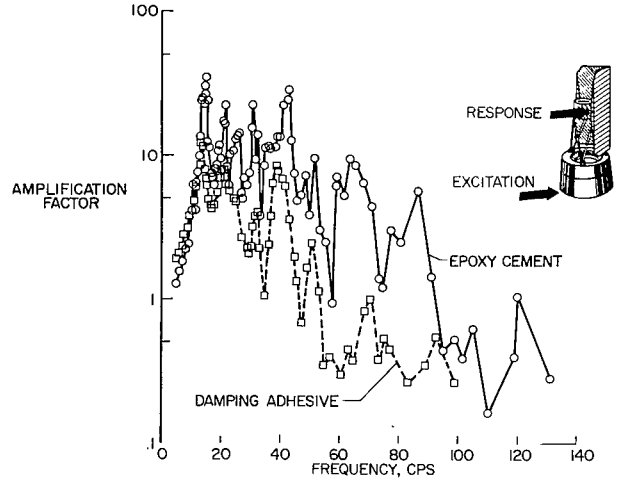

(c) Response at end of panel shaft.

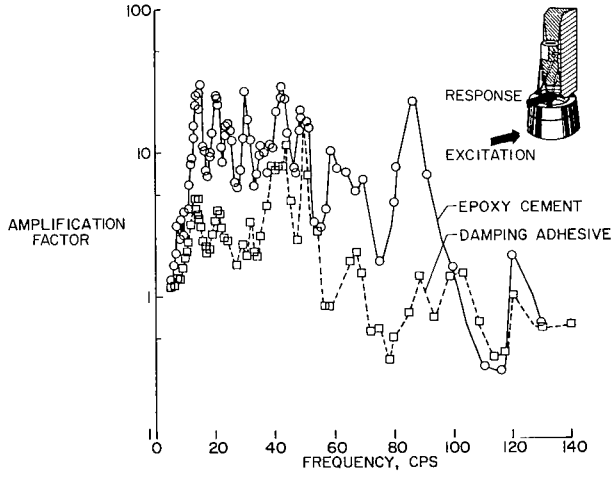

(b) Response at bottom of hinge line on panel transition.

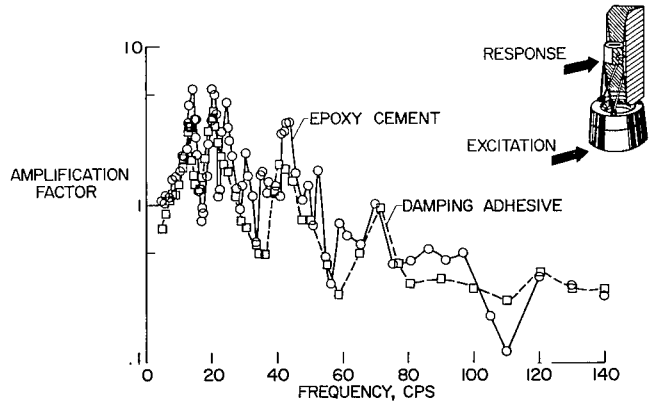

(d) Response at base of control section.

Figure 14.- Dynamic amplification as a function of excitation frequency of the 1/2-scale model; excitation is along roll axis. k = 15,250 lb/in.

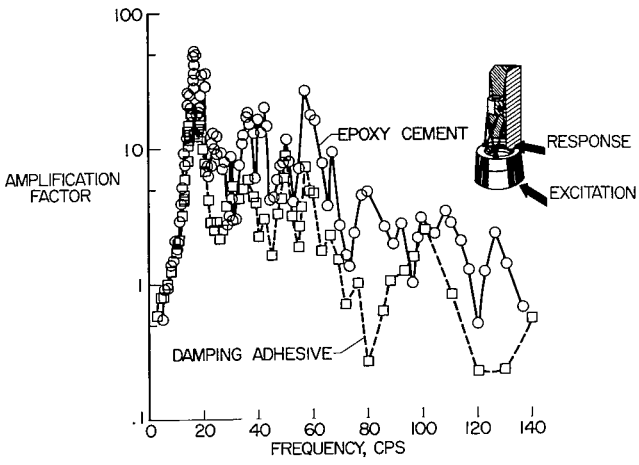

(a) Response at bottom center of solar panel.

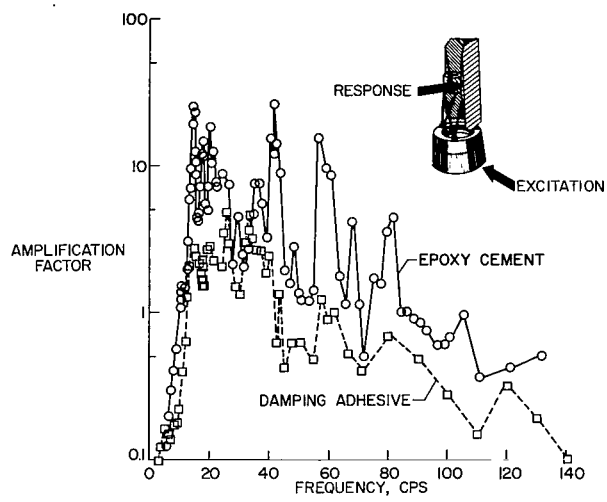

(b) Response at end of panel shaft.

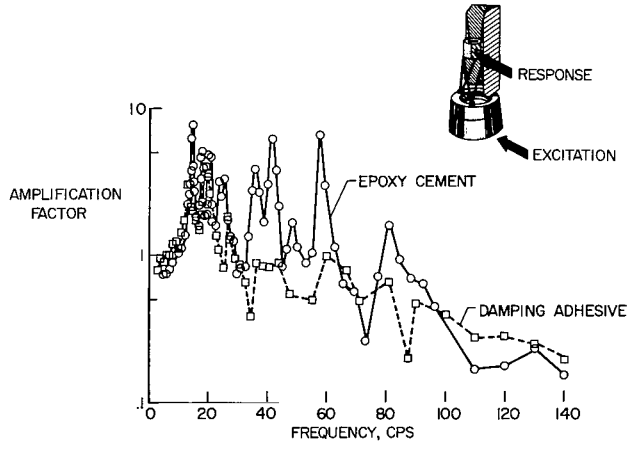

(c) Response at base of control section.

Figure 15.- Dynamic amplification as a function of excitation frequency of 1/2-scale model; excitation is along pitch axis. k = 15,250 lb/in.

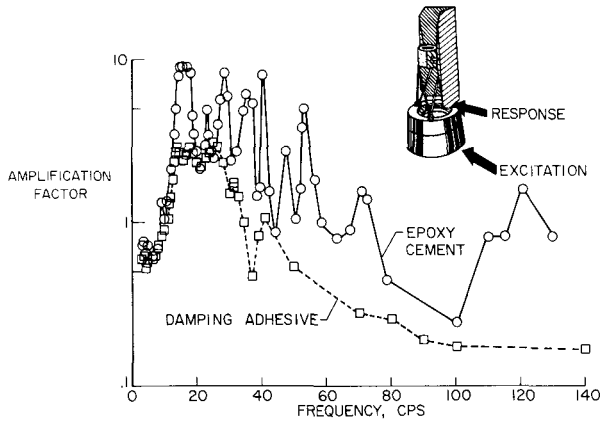

(a) Response at bottom center of solar panel.

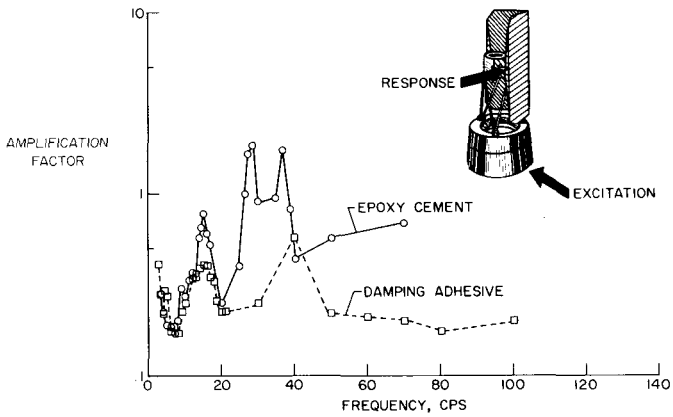

(b) Response at end of panel shaft.

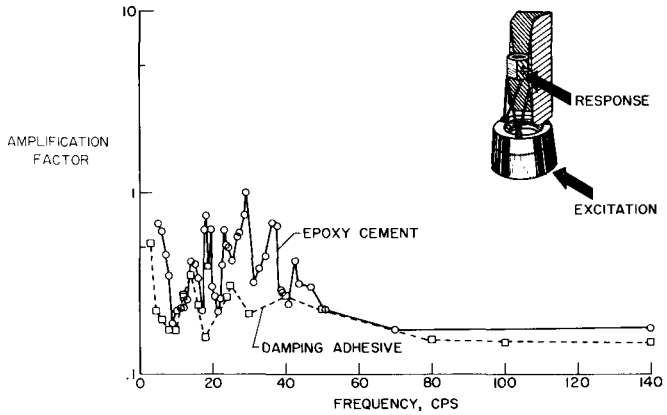

(c) Response at base of control section.

Figure 16.- Dynamic amplification as a function of excitation frequency; excitation is along pitch axis. Two isolators had a capacity from $5\frac{1}{2}$ to $12\frac{1}{2}$ lb; one had a capacity of 20 lb.

The results indicated that the isolation mounts were more effective in reducing magnitudes of structural amplification on the epoxy-bonded panels than were the inherently damped sandwich panels. The combination of both isolation mounts and the damped adhesive-bonded panels was extremely effective in reducing the magnitude of detectable structural resonances.

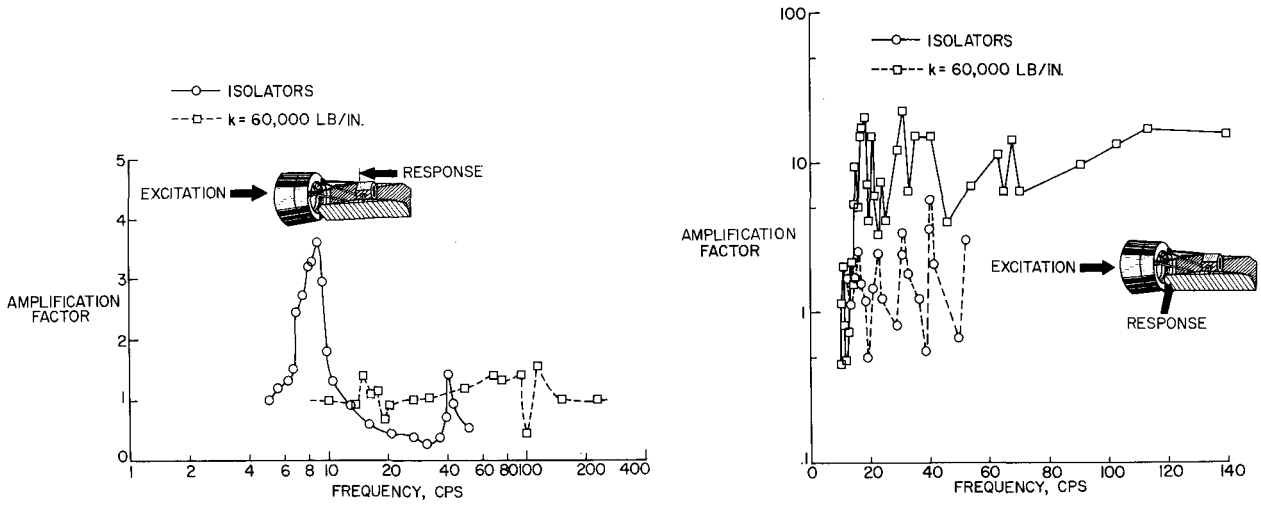

(a) Response at base of control section.

(b) Response at bottom center of epoxy-bonded solar panel.

Figure 17.- Dynamic amplification as a function of excitation frequency; excitation is along yaw axis.

For excitation along the yaw axis (fig. 17), amplification factors were determined for locations on the base of the control section and on the bottom center of the solar panel. The response of the model for k = 60,000 lb/in. between the control and sensory sections was used for comparison with the response for cases in which the isolation mounts were used. The results of these tests are presented in figure 17. For the location on the control section (fig. 17(a)), the amplification factor as a function of frequency was the typical mass-on-isolator response curve with attenuation occurring at frequencies above approximately 1.4 times the natural frequency of the mass-isolator system. As shown in the figure, the measured attenuations on the control section are essentially unity for k = 60,000 lb/in. Presented in figure 17(b) are the responses on the bottom center of the epoxy-bonded panels. Appreciable but somewhat less effectiveness was obtained through the use of the isolation mounts for responses at this location on the model.

Although the results indicate that reductions in the structural amplifications can be obtained by utilizing vibration isolation mounts, several disadvantages were also presented. One such undesirable feature is that large lateral movements, because of rocking action of the panels, control section, and struts, on the isolators can occur at the natural frequency of the isolators.

This fact presents the additional complication of possible interference of the model or vehicle panels with the launch-vehicle shroud. Further, for omnidirectional isolators to provide desired isolation, large deflections are often necessary. The deflections are needed to prevent bottoming of the isolators under the loading imposed by the increasing acceleration of the launch vehicle during the flight. Sacrifice of omnidirectional isolation for unidirectional isolation could possibly overcome some of the disadvantages.

Effects of stiffness between control and sensory sections.- To assess the effects on the response of the model of stiffness between the control and the sensory section, structural amplifications as a function of frequency were determined for values of k equal to 60,000 lb/in. and 15,250 lb/in. The results of this study are presented in figure 18, which shows the measured

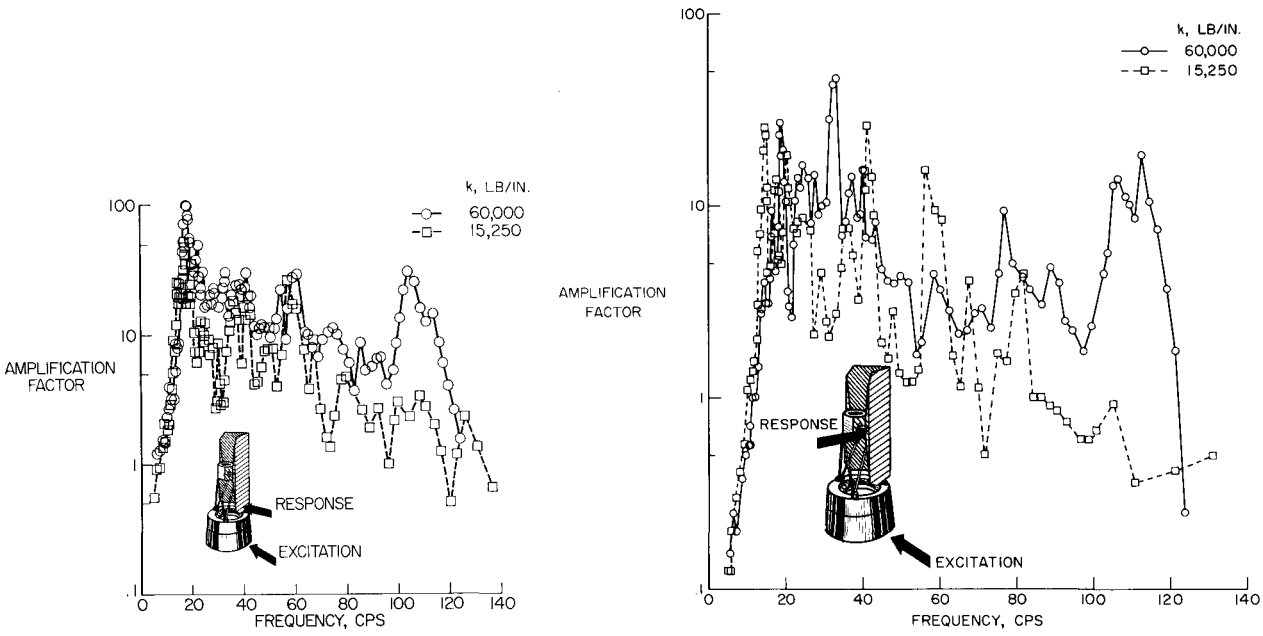

(a) Response at bottom center of solar panel.

(b) Response at end of panel shaft.

Figure 18.- Effects of stiffness between control and sensory sections on dynamic amplification of epoxy-bonded panels. Excitation is along pitch axis.

model response to inputs along the pitch axis for locations at the bottom center of the solar panel and at the end of the panel shaft. The results indicate that increased stiffness between the two sections leads to only slight increases in panel amplifications at somewhat increased frequencies.

Sensory-section response.- As might be intuitively expected, few, if any, reductions in the measured response in the compartments of the sensory section were noted when changes were made in the structure above the sensory section. As an illustration of the responses that occurred around the sensory section,

peak values of the amplifications in several compartments were measured and are presented in figure 19. Maximum structural amplifications were found to occur at or near the natural frequencies of the compartment panel, with the overall amplification magnitudes being less severe than these maximums.

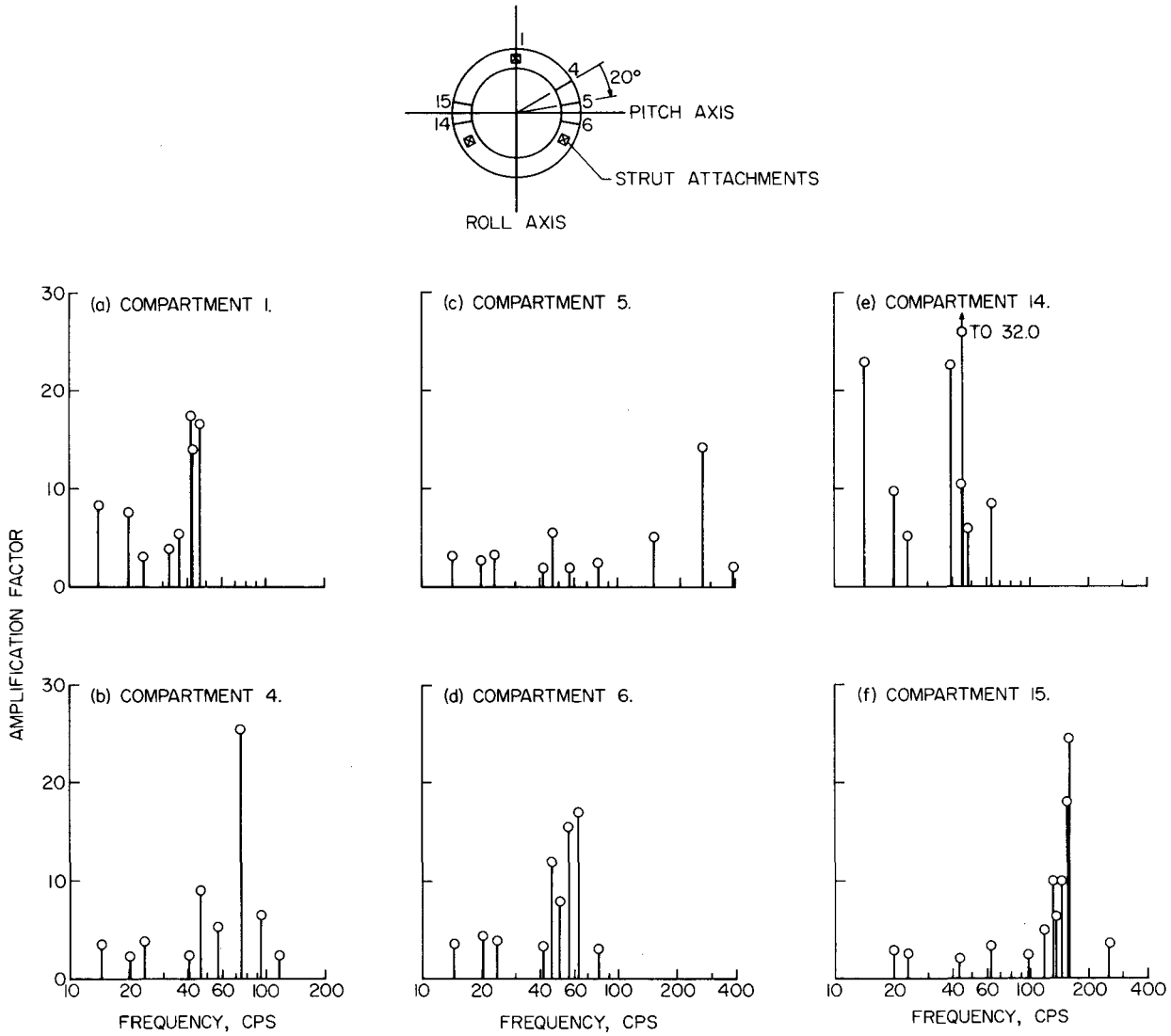

Figure 19.- Peak values of dynamic amplification as a function of excitation frequency for several sensory-section compartments; excitation is along roll axis.

CONCLUDING REMARKS

An investigation has been conducted to evaluate the effectiveness of various damping and isolation methods in reducing the structural amplifications of vibratory inputs on simplified models of the Nimbus spacecraft. The results are summarized in the following paragraphs:

1. Preliminary tests with a 1/5-scale model of the Nimbus spacecraft indicated potential vibration problems which should be explored with more detailed models of the spacecraft. The results also indicated that appreciable reductions in the magnitude of the structural resonances could possibly be realized through the use of appropriate damping and/or isolation.

2. Experimental frequencies for the first 10 modes of the solar panels on the 1/2-scale model were compared with calculated values using a finite-difference method. In general, good agreement between the calculated and experimental frequencies was found. Good agreement was also shown between the computed and experimental node locations.

3. A comparison between the responses of the 1/2-scale model and the full-scale vehicle at the base of the control section for inputs along the pitch axis indicated that general agreement existed between resonances of the model and the full-scale vehicle in the frequency range up to approximately 35 cps.

4. In the evaluation of the effects of distributed damping in the solar panels, the results emphasized (a) that very high amplifications exist in such structures; (b) that the many structural resonances were associated mainly with the natural modes of the panels; (c) that the response of such a structure to unsteady forces can be substantially reduced, with only a modest weight increase, by the use of damping materials at suitably chosen points.

5. Isolation mounts were more effective in reducing the magnitude of structural amplifications on the epoxy-bonded lightly damped solar panels than were the inherently damped panels. The combination of both isolation mounts and damped panels was extremely effective in reducing the magnitude of detectable structural resonances.

6. Increased stiffness between the control section and the sensory section resulted in only slight increases in panel amplifications at somewhat increased frequencies.

7. Little, if any, reductions in the measured response in the compartments of the sensory section were noted when changes were made in the structure above the sensory section.

Langley Research Center,
National Aeronautics and Space Administration,
Langley Station, Hampton, Va., May 19, 1964.

REFERENCES

1. Crede, Charles E.: Application and Design of Isolators. Data Analysis, Testing, and Methods of Control. Vol. 2 of Shock and Vibration Handbook, Cyril M. Harris and Charles E. Crede, eds., McGraw-Hill Book Co., Inc., 1961, pp. 32-1 - 32-53.

2. Walton, William C., Jr.: Applications of a General Finite-Difference Method for Calculating Bending Deformations of Solid Plates. NASA TN D-536, 1960.

3. Lazan, B. J., and Goodman, L. E.: Material and Interface Damping. Data Analysis, Testing, and Methods of Control. Vol. 2 of Shock and Vibration Handbook, Cyril M. Harris and Charles E. Crede, eds., McGraw-Hill Book Co., Inc., 1961, pp. 36-1 - 36-46.

4. Hamme, Richard N.: Vibration Control by Applied Damping Treatments. Data Analysis, Testing, and Methods of Control. Vol. 2 of Shock and Vibration Handbook, Cyril M. Harris and Charles E. Crede, eds., McGraw-Hill Book Co., Inc., 1961, pp. 37-1 - 37-34.

NASA-Langley, 1964 L-3744

2 17 / 85

"The aeronautical and space activities of the United States shall be conducted so as to contribute . . . to the expansion of human knowledge of phenomena in the atmosphere and space. The Administration shall provide for the widest practicable and appropriate dissemination of information concerning its activities and the results thereof."

—NATIONAL AERONAUTICS AND SPACE ACT OF 1958

NASA SCIENTIFIC AND TECHNICAL PUBLICATIONS

TECHNICAL REPORTS: Scientific and technical information considered important, complete, and a lasting contribution to existing knowledge.

TECHNICAL NOTES: Information less broad in scope but nevertheless of importance as a contribution to existing knowledge.

TECHNICAL MEMORANDUMS: Information receiving limited distribution because of preliminary data, security classification, or other reasons.

CONTRACTOR REPORTS: Technical information generated in connection with a NASA contract or grant and released under NASA auspices.

TECHNICAL TRANSLATIONS: Information published in a foreign language considered to merit NASA distribution in English.

TECHNICAL REPRINTS: Information derived from NASA activities and initially published in the form of journal articles.

SPECIAL PUBLICATIONS: Information derived from or of value to NASA activities but not necessarily reporting the results of individual NASA-programmed scientific efforts. Publications include conference proceedings, monographs, data compilations, handbooks, sourcebooks, and special bibliographies.

Details on the availability of these publications may be obtained from:

SCIENTIFIC AND TECHNICAL INFORMATION DIVISION

NATIONAL AERONAUTICS AND SPACE ADMINISTRATION

Washington, D.C. 20546